Nuclear Materials and Energy 34 (2023) 101364

Contents lists available at ScienceDirect

Nuclear Materials and Energy

journal homepage: www.elsevier.com/locate/nme

Inverse change in positron lifetimes of vacancies in tungsten by binding of interstitial impurity atoms to a vacancy: A first-principles study

Atsushi Yabuuchi

Institute for Integrated Radiation and Nuclear Science, Kyoto University, Kumatori, Osaka 590–0494, Japan

ARTICLE INFO

Keywords:
First-principles calculation
Defect complex
Binding energy
Positron annihilation spectroscopy
Positron lifetime

ABSTRACT

First-principles calculations related to defect complexes formed from a monovacancy and multiple interstitial impurity atoms (hydrogen, carbon, nitrogen, and oxygen atoms) in tungsten were performed. The most stable atomic configurations, the electron density distributions, the binding energies of impurity atoms, and the positron lifetimes of each defect complex were calculated. In calculating positron lifetimes, slight deviations in the initial positions of the H atoms were found to be enhanced by positron localization, which affected the positron lifetimes of the vacancy-hydrogen complexes. In addition, the positron lifetimes of vacancy-nitrogen and vacancy-oxygen complexes were found to become longer in some cases with increasing numbers of impurity atoms that bound to the vacancy. Such longer positron lifetimes with increasing numbers of binding impurity atoms were attributed to the fact that the impurity atoms bind slightly further away from the vacancy, expanding the tungsten lattice.

1. Introduction

Positron annihilation spectroscopy is useful for detecting vacancy-type defects in crystalline materials [1–4]. Fig. 1 shows examples of calculated positron density distributions in a defect-free bulk tungsten lattice and a tungsten lattice containing a monovacancy. In crystalline materials, positrons are repelled from nuclei and spread to interstitial positions, while in the presence of a vacancy, they are localized in the vacancy. Since positrons eventually annihilate with electrons in crystals and emit annihilation gamma rays, one can observe the positron lifetimes in crystalline materials. The positron lifetime contains information on the electron density around positrons, thus measuring the positron lifetimes makes it possible to investigate vacancies in crystalline materials [1–4].

Because of the superior properties of positrons in characterizing vacancy-type defects, as described above, positron annihilation lifetime spectroscopy is widely used to study tungsten (W), a plasma-facing material in fusion reactors that must withstand neutron and plasma irradiation [4]. In characterizing vacancies in metals using positron annihilation lifetime measurements, defect species (e.g., vacancies associated with dislocations, isolated monovacancies, divacancies, or larger vacancy clusters) are often discriminated based on the difference in positron lifetimes. However, when the vacancy is bound with an interstitial impurity atom such as hydrogen (H), carbon (C), nitrogen (N), or oxygen (O), the positron lifetime of the defect changes significantly. These light-element impurities are difficult to remove from the metal completely, and they are often not included in the purity analysis of metals. For example, although light-element impurities evaporate to some extent during the manufacturing process, sintered W still contains H, C, N, and O atoms at concentrations on the order of wt ppm [5]. Because of the heavy atomic weight of W (~184), the wt% concentration of H in W becomes around 200 times when converted to at%, and more than 10 times higher for C, N, and O as well. These interstitial impurity atoms have large attractive interactions with vacancies [6] and significantly influence the thermal behavior of vacancies in W. In particular, H and O atoms have been reported to have small migration energies of 0.21 eV and 0.17 eV, respectively, in W [7,8]. This means that H and O atoms can diffuse over a distance of the order of 10 μm in a second, even at the relatively low temperature of 100 °C [6], where vacancies hardly migrate. Hence, a large number of extrinsic H and/or O atoms may be incorporated into the W crystal, and multiple H and/or O atoms are expected to bind to one vacancy. It is important to preliminarily evaluate the effects of these interstitial impurity atoms on the positron lifetimes to study vacancy-type defects in W using positron annihilation lifetime spectroscopy.

In this study, first-principles calculations investigated the change in the positron lifetime of a monovacancy bound with multiple H, C, N, or O atoms in W. As a result, the H atoms bound to a vacancy were found to be largely displaced with positron localization. In addition, the changes in the positron lifetime were found to show different trends in the case of H and C atoms and in the case of *N* and O atoms. As preliminary calculations, the most stable atomic configurations, the

E-mail address: yabuuchi@rri.kyoto-u.ac.jp.

https://doi.org/10.1016/j.nme.2023.101364
Received 24 August 2022; Received in revised form 17 December 2022; Accepted 9 January 2023
Available online 13 January 2023

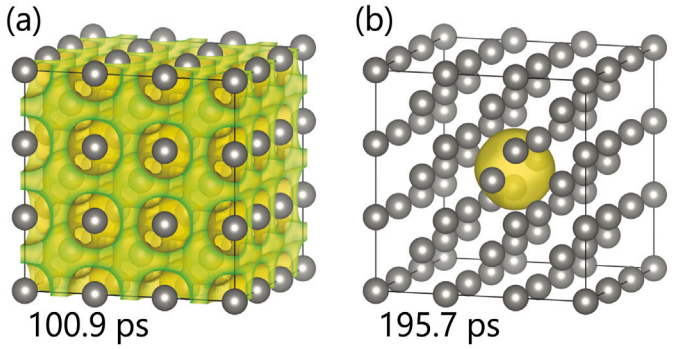

Fig. 1. Calculated positron density distributions for (a) a defect-free bulk tungsten lattice and (b) a tungsten lattice containing a monovacancy. The calculated positron lifetimes obtained in this study are also indicated at the bottom of each panel. Note that the positron density distribution of the defect-free bulk tungsten lattice, where a positron is delocalized, is emphasized compared with that of the vacancy-containing tungsten lattice.

electron density distributions, and the binding energies of impurity atoms were calculated.

2. Computational method

Vacancy formation energy, binding energies of an interstitial impurity atom to a vacancy (or vacancy-impurity complex), positron lifetimes, and DBAR spectra were calculated using ABINIT [9–11], a program based on density functional theory (DFT). The electron–ion interaction was modeled using the projector augmented-wave method of Blöchl [12,13]. The exchange–correlation functional between electrons was described using the generalized gradient approximation of Perdew, Burke, and Ernzerhof [14]. Positron lifetimes were calculated using a two-component DFT scheme [15,16], which considers the effect of positron localization on the electron density distribution, with the local density approximation of Puska, Seitsonen, and Nieminen as the electron-positron exchange–correlation functional [17]. The calculations were performed using body-centered cubic supercells with a size of 3 × 3 × 3, as shown in Fig. 1, i.e., containing 54 atoms in the defect-free W bulk. The plane-wave cutoff energy and k-point sampling mesh were 408 eV and a 6 × 6 × 6 mesh, respectively. The atomic configurations of all defect structures were optimized by iterating lattice relaxation calculations until the forces acting on each atom in the supercell became less than 0.01 eV/Å. When a positron localizes at a vacancy, the electron density around the vacancy varies [15], and the force acting on each atom around the vacancy also varies [18]. This causes lattice relaxation around the vacancy by trapping a positron into the vacancy, which will also affect the positron lifetime. Thus, in calculating positron lifetimes, the lattice relaxation calculations were iterated again until the force acting on each atom around the vacancy where a positron is localized became less than 0.01 eV/Å. The atomic configurations, electron density distributions, and positron density distributions were plotted using the VESTA program [19].

To confirm that the obtained value is comparable to those reported in other studies, the formation energy of an isolated monovacancy in W, E_V^{F}, was calculated from the following equation:

$$E_V^{\mathrm{F}} = E\left(\mathrm{W}_{n-1}V\right) - \frac{n-1}{n}E\left(\mathrm{W}_n\right), \tag{1}$$

where, n is the number of W atoms in the defect-free bulk supercell (n = 54 in this study). $E\left(\mathrm{W}_n\right)$ and $E\left(\mathrm{W}_{n-1}V\right)$ are the total energies of the supercells for the defect-free bulk and isolated monovacancy, respectively. The binding energies $E^{\mathrm{B}}_{V\mathrm{H}_k}$ between a vacancy-hydrogen complex bound with $(k-1)$ H atoms ($V\mathrm{H}_{k-1}$) and the kth H atom were defined by the following equation:

$$E^{\mathrm{B}}_{V\mathrm{H}_k} = \left\{ E\left(\mathrm{W}_{n-1}V\mathrm{H}_{k-1}\right) + E\left(\mathrm{W}_n\mathrm{H}^{\mathrm{I}}\right) \right\}$$

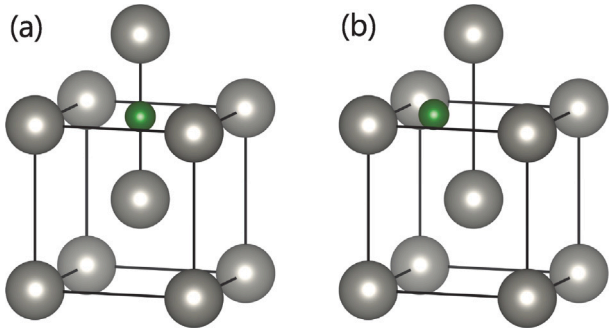

Fig. 2. Two candidate positions for isolated interstitial impurity atom: (a) O-site and (b) T-site. Note that lattice relaxation is not reflected in the plots of the atomic configurations in this figure.

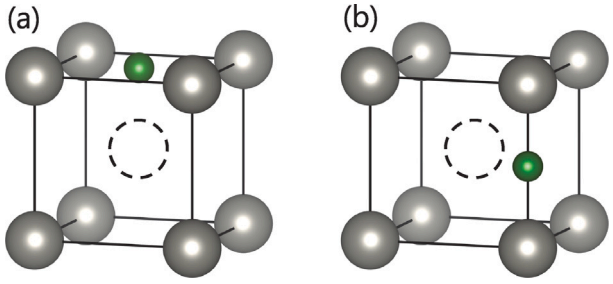

Fig. 3. Interstitial impurity atom located at the (a) 1NN and (b) 2NN O-sites from the vacancy. Note that lattice relaxation is not reflected in the plots of the atomic configurations in this figure.

$$- \left\{ E\left(\mathrm{W}_{n-1}V\mathrm{H}_k\right) + E\left(\mathrm{W}_n\right) \right\}, \tag{2}$$

where, $E\left(\mathrm{W}_{n-1}V\mathrm{H}_k\right)$, $E\left(\mathrm{W}_{n-1}V\mathrm{H}_{k-1}\right)$, and $E\left(\mathrm{W}_n\mathrm{H}^{\mathrm{I}}\right)$ are the total energies of the supercells for the $V\mathrm{H}_k$, $V\mathrm{H}_{k-1}$, and an isolated interstitial H atom, respectively. This study performed calculations for k in the range of 1 to 6. There are two candidates for the position of the isolated interstitial hydrogen atom H^{I}, i.e., an octahedral-site (O-site) and a tetrahedral-site (T-site), as shown in Fig. 2. The total energies $E\left(\mathrm{W}_n\mathrm{H}^{\mathrm{I}}\right)$ were determined for calculating both the total energies of the H^{I} placed at the O-site or at the T-site, to investigate the more stable position of H^{I}. The binding energies of the C, N, and O atoms were also defined and calculated in the same manner as above.

The most stable atomic configuration of each defect must be investigated to calculate the binding energy of an impurity atom to a vacancy (or a vacancy-impurity complex) and the positron annihilation characteristics at that defect. In this study, lattice relaxation calculations were performed with the O-site around the vacancy as the initial position of each interstitial impurity atom. Then, the final atomic configurations were determined. The T-sites were not used as the initial positions except for the $V\mathrm{H}_k$ calculations because the interstitial impurity atom around the vacancy eventually moved to the most stable position regardless of whether the interstitial impurity atom was initially placed at the O-site or T-site. There was first nearest neighbor (1NN) O-sites and second nearest neighbor (2NN) O-sites around a vacancy, as shown in Fig. 3. The 1NN and 2NN O-sites were present around the vacancy with 6 and 12 locations, respectively. Furthermore, in the case of $k \geq 2$, multiple O-sites were the possible candidates for the configuration of the kth interstitial impurity atom, based on the positional relationship with the $k-1$ interstitial impurity atoms that were already bound to the vacancy. Lattice relaxation calculations were performed for all possible atomic configurations with 1NN or 2NN O-sites as the initial positions of the interstitial impurity atom, and the most stable atomic

Table 1
Energy difference (in eV) from the stable site of each isolated interstitial atom. The sites indicated as 0 are the stable sites for each element.

Element	O-site	T-site
H	+0.41	0
C	0	+1.65
N	0	+0.95
O	+0.10	0

configuration for each defect was determined by comparing their total energies.

In consideration of the zero-point energy (ZPE), the equilibrium position of the H atom bound to a vacancy has been reported to slightly deviate from the straight line connecting the 1NN O-site and the vacancy center [20,21]. Although the ZPE correction was not taken into account in this study, lattice relaxation calculations for the VH_k defect complexes were also performed with the T-sites as the initial positions of the H atoms in order to reproduce the slight deviation of the H atoms. The positional relationships of multiple initial T-sites when $k \geq 2$ were determined based on Fig. 10 in Ref. [20].

3. Results and discussion

3.1. Atomic configurations

The vacancy formation energy E_V^F in tungsten obtained from Eq. (1) was 3.65 eV. This value is comparable to experimental (3.51–4.0 eV) [22–24] and calculated (3.14–3.95 eV) [7,25–30] values reported in other studies.

Table 1 shows whether the stable site of each isolated impurity atom was the O- or T-site, and the energy difference between the O- and T-sites. The site indicated by 0 in the table is the stable site for each element. The calculations in this study showed that the H and O atoms were more stable at the T-site, while the C and N atoms were more stable at the O-site. These obtained stable sites are consistent with the results reported in other studies [7,8,25,30–33]. This result that the energy difference between the O- and T-sites was large for C and N atoms and relatively small for H and O atoms is also similar to that reported in other studies [7,8,30].

Then, the most stable atomic configurations of the VH_k, VC_k, VN_k, and VO_k defect complexes ($k \leq 6$) are discussed. The obtained atomic configurations are shown in Fig. 4. The positions of the atoms are plotted in the figure, considering lattice relaxation.

3.1.1. Vacancy-hydrogen complexes

The top row of Fig. 4 shows the most stable atomic configurations of the VH_k defect complexes. These were obtained by performing lattice relaxation calculations with T-sites as the initial positions of H atoms. Fig. 4 shows that the first H atom was located near the 1NN O-site. The second H atom was located at the 1NN O-site, opposite the first H atom. The third H atom was located at the 1NN O-site, at 90 degrees to the first and second H atoms. The three H atoms were aligned on the {100} plane. The fourth H atom was located at the 1NN O-site, where the fourth H atom formed a tetrahedron. The fifth H atom was located at the 1NN O-site, where the fifth H atom formed a square pyramid. Finally, the sixth H atom was located at the 1NN O-site, where the sixth H atom formed an octahedron.

Fig. 5 compares the structures with H atoms relaxed from the 1NN O-sites and the structures with H atoms relaxed from the T-sites. In the VH_1, the H atom that was relaxed from the 1NN O-site was displaced straight toward the vacancy center by $\sim 0.1a$ (a is the lattice constant of W). In contrast, the H atom relaxed from the T-site satisfied the convergence condition for the force acting on each atom (< 0.01 eV/Å) at a position deviating by $\sim 0.04a$ from the straight line connecting the 1NN O-site and the vacancy center. The structure of the obtained VH_1 defect complex is generally similar to that of VH_1 reported by Ohsawa et al. [20]. Similarly, for the VH_2 to VH_5 defect complex, the positions of the H atoms relaxed from the T-site were slightly shifted compared to those relaxed from the 1NN O-site. (However, the third H atom of the VH_3 was shifted in the [100] direction, which is not visible in Fig. 5.) On the other hand, the VH_6 defect complex was found to be significantly more stable when the H atoms were relaxed from the T-sites than when they were relaxed from the 1NN O-sites. Fig. 5 indicates that the H atoms relaxed from the T-sites in the VH_6 are displaced significantly compared with those relaxed from the 1NN O-sites.

Since the ZPE correction was not taken into account in this study, in the case of the VH_1 and VH_2, the energy differences between the structures with and without the deviation of the H atoms shown in Fig. 5 are negligible (< 1 meV). In the case of the VH_3 to VH_5, the structures with the H atoms relaxed from the T-sites were slightly (~0.01 eV) more stable. In contrast, in the case of the VH_6, the structure with the H atoms relaxed from the T-sites was found to be energetically more stable by 0.31 eV than the structure with the H atoms relaxed from the 1NN O-sites.

The obtained atomic configurations of VH_k shown in Fig. 4 are consistent with those reported in past studies [20,21,34]. On the other hand, Liu et al. [25] proposed a planar configuration (like VC_4 in Fig. 4) as the most stable atomic configuration of VH_4. However, in the calculations of this study, VH_4, in which four H atoms formed a tetrahedron, as shown in Fig. 4, was energetically more stable than the planar VH_4, by 0.16 eV.

3.1.2. Vacancy-carbon complexes

As in the case of the H atom, the first C atom was located near the 1NN O-site. Unliken the H atom, the second C atom was not located at the 1NN O-site, opposite the first C atom, but it was located at the 1NN O-site at 90 degrees to the first C atom. The third C atom was located at the 1NN O-site, opposite the first C atom. The fourth C atom was located at the 1NN O-site, opposite the second C atom, and the four C atoms were aligned on the {100} plane. When located at the 2NN O-site, the fifth C atom was more stable than at the 1NN O-site. However, the calculations showed that the fifth C atom was repulsive (i.e., the binding energy between the VC_4 and the fifth C atom was negative), therefore, the calculation of the VC_6 defect complex was not performed.

The atomic configurations of VC_k obtained from the present calculations were consistent with those reported by Kong et al. [30]. The atomic configurations of VC_k suggested the attractive interaction between C atoms around a vacancy. For example, in the VC_4 and VH_4 defect complexes, the minimum interatomic distance of C–C was only 77% compared with that of H–H.

3.1.3. Vacancy-nitrogen complexes

In the case of VN_k, the atomic configurations were the same as for VH_k up to $k \leq 2$. For $k \geq 3$, the third, fourth, fifth, and sixth N atoms were all located at the 2NN O-site rather than the 1NN O-site. The three N atoms in the VN_3 and the four N atoms in the VN_4 were both aligned on the {110} plane. The atomic configurations of the VN_k were consistent with those reported by Kong et al. [30].

In contrast to the case of C atoms, repulsive interaction between N atoms around a vacancy was suggested from the atomic configurations of VN_k. For example, the minimum interatomic distance of N–N in VN_4 was 136% compared with that of H–H in VH_4. Furthermore, since the third and subsequent N atoms were located at the 2NN O-site, the distance between the W–W atoms was expanded. In the VN_6, the W–W interatomic distance in the ⟨100⟩ direction with an N atom in between became 118% compared with that in defect-free bulk W.

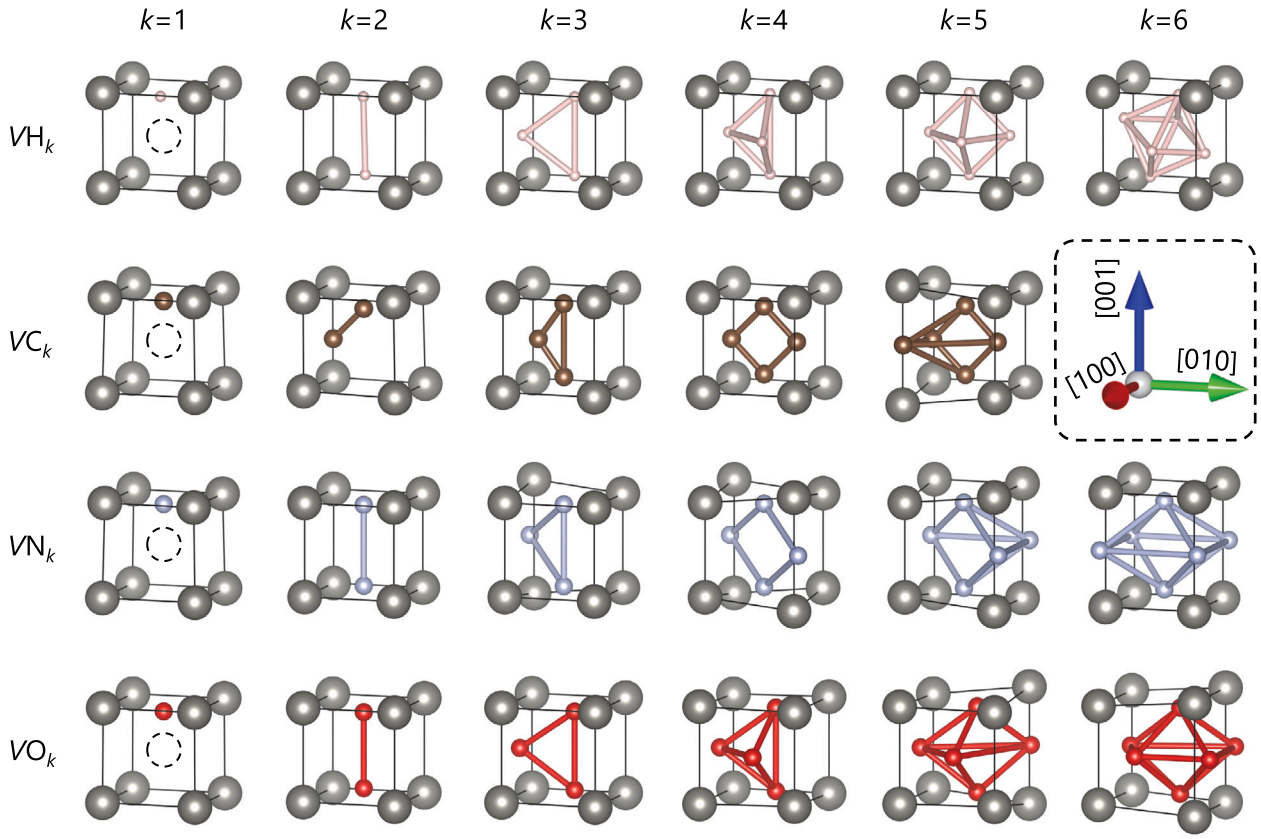

Fig. 4. Most stable atomic configurations of the VH_k, VC_k, VN_k, and VO_k defect complexes ($k \leq 6$). The positions of the atoms are plotted with consideration of lattice relaxation. The impurity atoms are connected to each other by cylinders to make it easier to see the positional relationship between impurity atoms. Broken circles representing a vacancy are omitted for $k \geq 2$.

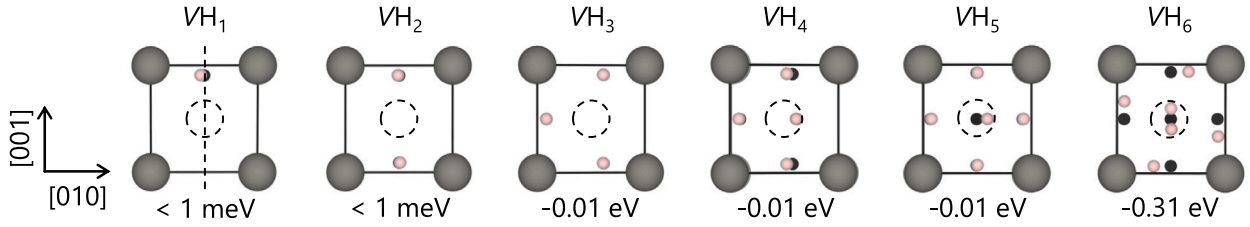

Fig. 5. Atomic configurations of the VH_k defect complexes when the H atoms are relaxed from the O- or T-sites. H atoms relaxed from the O- and T-sites are drawn in black and pink, respectively. A dashed line connecting the 1NN O-site and the vacancy center is also depicted in the VH_1 panel. The values at the bottom of each panel show the difference in total energy between the structure with H atoms relaxed from the T-sites and that with H atoms relaxed from the 1NN O-sites.

3.1.4. Vacancy-oxygen complexes

In the case of VO_k, the atomic configurations were the same as for VH_k up to $k \leq 4$. Unlike the case of VH_k, the fifth O atom was located at the 2NN O-site. The sixth O atom was placed at the 1NN O-site as the initial structure of the calculation. Through the lattice relaxation calculation, the sixth O atom was eventually located near the T-site.

In the case of VO_k, the fifth O atom was also located at the 2NN O-site, thus expanding the interatomic distance of W–W. In the VO_5, the interatomic distance of W–W in the ⟨100⟩ direction with an O atom in between was 121% compared with that of the defect-free bulk.

3.2. Electron density distributions

The electron density distributions on the (100) plane of each defect complex shown in Fig. 4 are presented in Fig. 6. The electron density distribution of the VC_5 is not shown because the binding energy between the VC_4 and the fifth C atom is negative (i.e., the VC_5 is not stable), as will be discussed later. Focusing on the dependence of the electron density distribution on impurity elements, it can be seen that only carbon has different characteristics from the other impurity elements. In the case of H, N, and O atoms, the electron density in the region between the impurity atoms did not increase even when the impurity atoms were close to each other. In contrast, an obvious increase in electron density was observed in the region between the C atoms. In the case of the VC_4, the region of low electron density has almost disappeared. On the other hand, in the case of the VN_k, a gradual expansion of the low electron density region was observed from VN_2 to VN_6. This is because the third and subsequent N atoms occupy the 2NN O-sites and expand the vacancy volume, as shown in Fig. 4.

To investigate charge transfer between the vacancy and the impurity atom, the difference electron density distributions of the VX_1 (X=H, C, N, and O) are plotted in Fig. 7. The difference electron density distribution was derived from the electron density distribution of the VX_1 by subtracting the sum of the electron density distributions when only W atoms were placed and when only the impurity atom X was placed. In the calculations of the difference electron density distributions, the positions of each atom were kept the same. The distances

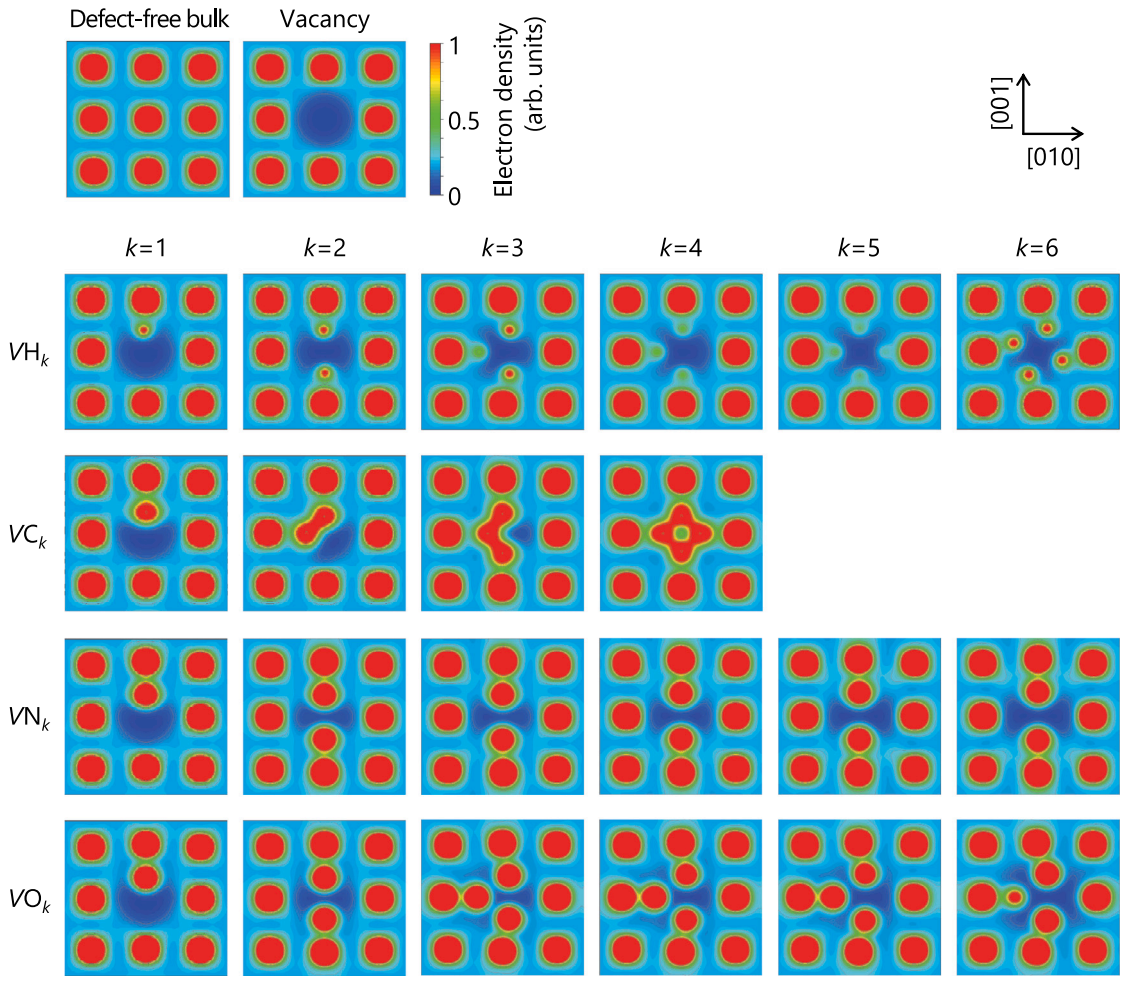

Fig. 6. Electron density distributions on the (100) plane through the vacancy center.

of H, C, N, and O atoms from the vacancy center in each $V\mathrm{X}_1$ defect complex were $0.41a$, $0.40a$, $0.43a$, and $0.43a$, respectively (where a is the lattice constant of W), and none of them were significantly different. In addition, the charge transfer around the vacancy due to the presence of each impurity atom was qualitatively similar for the four impurity elements. Therefore, the difference in the atomic configurations of the impurity atoms around the vacancy, depending on the impurity elements, seems to be due to the difference in the interaction between the impurity atoms rather than to the difference in the interaction between the impurity atom and the vacancy.

3.3. Binding energies

The binding energies $E^{\mathrm{B}}_{V\mathrm{X}_k}$ of the $V\mathrm{X}_{k-1}$ defect complex and the kth isolated X atom (X=H, C, N, and O) calculated based on Eq. (2) are shown in Fig. 8. Except for $E^{\mathrm{B}}_{V\mathrm{C}_5}$, the $E^{\mathrm{B}}_{V\mathrm{X}_k}$ shown in Fig. 8 was positive, indicating that each impurity atom could bind up to at least 6 in one vacancy, except for the C atom.

The present calculations showed that the binding energy between an isolated monovacancy and an isolated H atom ($E^{\mathrm{B}}_{V\mathrm{H}_1}$) was 1.13 eV, which is comparable to the binding energy of 1.18 eV reported by Liu et al. [25]. With increasing k, the binding energy between the $V\mathrm{H}_{k-1}$ defect complex and the kth H atom decreased gradually, and the binding energy of the sixth H atom became 0.59 eV. Liu et al. [25] have reported that the binding energies of the fourth and fifth H atoms were 0.70 and ~1.1 eV, respectively. This large variation in binding energies may be due to the fact that Liu et al. [25] adopted a metastable planar atomic configuration as the defect structure of the $V\mathrm{H}_4$ in their binding energy calculations, rather than the more stable atomic configuration (tetrahedral structure as shown in Fig. 4). In the present calculations, the binding energies of the fourth and fifth H atoms were 0.88 and 0.84 eV, respectively.

The binding energies of the first C and N atom to an isolated monovacancy ($E^{\mathrm{B}}_{V\mathrm{C}_1}$ and $E^{\mathrm{B}}_{V\mathrm{N}_1}$) were 1.97 and 2.46 eV, respectively. The binding energy $E^{\mathrm{B}}_{V\mathrm{C}_k}$ of the kth C atom to the $V\mathrm{C}_{k-1}$ defect complex, up to $k \leq 4$, was positive and turned negative at $k = 5$. When k increased from 2 to 3, the binding energy $E^{\mathrm{B}}_{V\mathrm{N}_k}$ of the kth N atom to the $V\mathrm{N}_{k-1}$ defect complex decreased significantly and did not change much at $3 \leq k \leq 6$. These tendencies in $E^{\mathrm{B}}_{V\mathrm{C}_k}$ and $E^{\mathrm{B}}_{V\mathrm{N}_k}$ are consistent with the calculations by Kong et al. [30].

The binding energy $E^{\mathrm{B}}_{V\mathrm{O}_k}$ of the kth O atom to the $V\mathrm{O}_{k-1}$ defect complex also showed the same tendency as $E^{\mathrm{B}}_{V\mathrm{N}_k}$, as shown in Fig. 8. That is, when k increased from 2 to 3 the $E^{\mathrm{B}}_{V\mathrm{O}_k}$ decreased significantly, and then it did not change much at $3 \leq k \leq 6$. This tendency was different from the reported interaction between a vacancy and O atoms in W calculated by Alkhamees et al. [35]. They also calculated binding energies using the same way as in Eq. (2) of the present study, and up to $k \leq 3$, obtained a result similar to the present study. However, they reported that the $V\mathrm{O}_3$ defect complex and the fourth O atom were repulsive. Although the atomic configuration of $V\mathrm{O}_4$ was not shown in their paper, the discrepancy in the binding energy of the fourth O atom may be attributed to the different atomic configurations of $V\mathrm{O}_4$ used in the calculations. Fig. 9(a) shows the atomic configuration of $V\mathrm{O}_4$ used in the binding energy calculation in Fig. 8, but if one instead uses a planar $V\mathrm{O}_4$ with four O atoms aligned on the {100} plane as shown

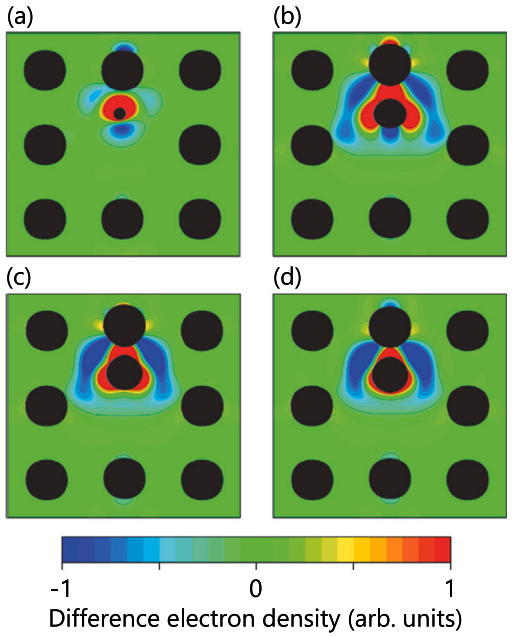

Fig. 7. Difference electron density distributions of the (a) $V\mathrm{H}_1$, (b) $V\mathrm{C}_1$, (c) $V\mathrm{N}_1$, and (d) $V\mathrm{O}_1$ defect complexes on the (100) plane through the vacancy center. Large and small black circles indicate the positions of W and impurity atoms, respectively.

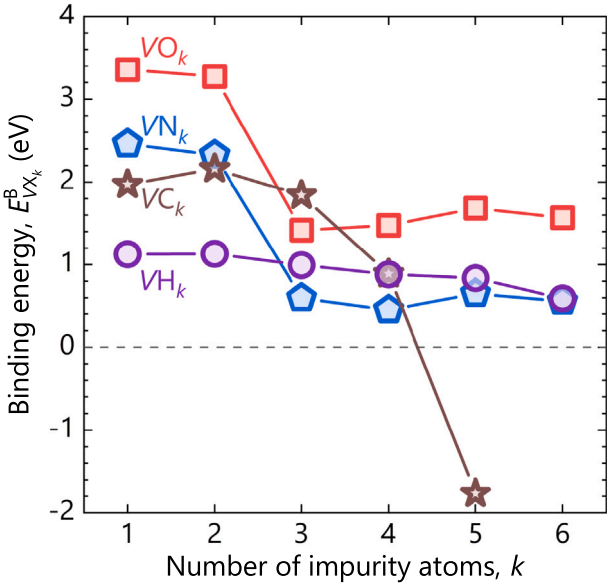

Fig. 8. Binding energies $E^{\mathrm{B}}_{V\mathrm{X}_k}$ of the kth isolated interstitial impurity atom to the $V\mathrm{X}_{k-1}$ (X=H, C, N, and O) defect complex. Positive and negative values represent attractive and repulsive interactions, respectively.

in Fig. 9(b), the binding energy of the fourth O atom would become −0.04 eV. Actually, the fourth O atom is also attractive because the atomic configuration shown in Fig. 9(a) is energetically more stable, by 1.52 eV compared to that shown in Fig. 9(b).

3.4. Positron lifetimes

The positron density distributions calculated in this study for defect-free bulk and isolated monovacancy are shown in Fig. 1. The calculated

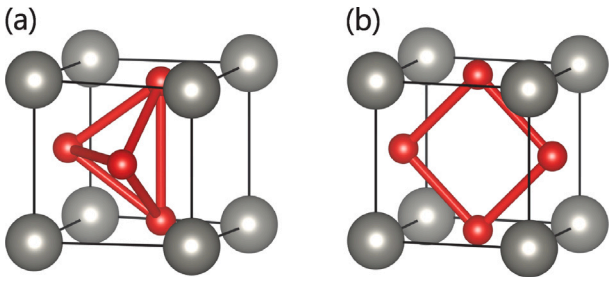

Fig. 9. Two different atomic configurations of $V\mathrm{O}_4$ defect complexes. (a) Tetrahedral structure; and (b) planar structure aligned on a {100} plane.

positron lifetimes for defect-free bulk and isolated monovacancy were 100.9 ps and 195.7 ps, respectively. These values are comparable to a previous study [6] and other studies [34,36,37]. Fig. 10 shows the positron density distributions and respective positron lifetimes in the $V\mathrm{H}_k$, $V\mathrm{C}_k$, $V\mathrm{N}_k$, and $V\mathrm{O}_k$ defect complexes calculated in this study. The k-dependence of the positron lifetimes for each defect complex is summarized in Fig. 11.

When a single H atom was bound to a monovacancy, the positron lifetime of the defect became shorter, from 195.7 ps to 186.3 ps. The calculated positron lifetime for the $V\mathrm{H}_2$ defect complex was 176.1 ps. Then, the positron lifetime of $V\mathrm{H}_k$ then continued to shorten monotonically up to $k = 6$, reaching 152.3 ps for $V\mathrm{H}_6$.

In the case of the $V\mathrm{H}_1$, as mentioned above, the H atom that relaxed from the T-site was located at a slightly deviated position ($\sim 0.04a$) from the straight line connecting the 1NN O-site and the vacancy center. This slight deviation of the H atom was found to be enhanced by the positron localization to the vacancy. Fig. 12 shows the lattice relaxations of the $V\mathrm{H}_k$ defect complexes due to the positron localization. In the $V\mathrm{H}_1$ where the H atom was relaxed from the 1NN O-site, a localized positron pushed the H atom straight out toward the 1NN O-site. In contrast, in the $V\mathrm{H}_1$ where the H atom was relaxed from the T-site, a localized positron pushed the H atom largely toward the T-site direction. As a result, the calculated positron lifetime became longer from 184.1 ps to 186.3 ps. Even in the $V\mathrm{H}_2$ where the H atoms were relaxed from the T-sites, the H atoms were displaced largely due to the positron localization, and the calculated positron lifetime elongated from 170.1 ps to 176.1 ps. The calculated positron lifetimes of the $V\mathrm{H}_3$, $V\mathrm{H}_4$, and $V\mathrm{H}_5$ where the H atoms were relaxed from the T-sites, were also elongated by a few ps. Furthermore, partly because the H atoms were largely displaced even before the positron localization, the calculated positron lifetime was significantly elongated from 134.1 ps to 152.3 ps in the $V\mathrm{H}_6$ where the H atoms were relaxed from the T-site.

Fig. 13 shows the relaxations due to the positron localization when C, N, and O atoms are located at the same initial position as the deviated H atom. (The stable positions of the C, N, and O atoms were actually closer to the 1NN O-site even when each impurity atom was relaxed from the T-site. In other words, the deviations from the straight line connecting the 1NN O-site and the vacancy center were about 1/10 of that for the H atom.) Even though the initial positions of the C, N, and O atoms were located at the same position as the deviated H atom, each impurity atom approached the 1NN O-site as a result of relaxation due to the positron localization, in contrast to the case of the H atom. The calculated positron lifetimes of the $V\mathrm{C}_1$, $V\mathrm{N}_1$, and $V\mathrm{O}_1$ obtained here were also almost the same as those for the structures in which each impurity atom was relaxed from the 1NN O-site shown in Fig. 10. This result indicates that in positron lifetime calculations for vacancy-hydrogen complexes, it should be noted that slight deviations in the initial positions of the H atoms are enhanced by positron localization, which also affects the positron lifetimes.

Then, the calculated positron lifetimes for vacancy-carbon complexes will be discussed. When a single C atom was bound to a monovacancy, the positron lifetime of the defect became shorter, from 195.7 ps

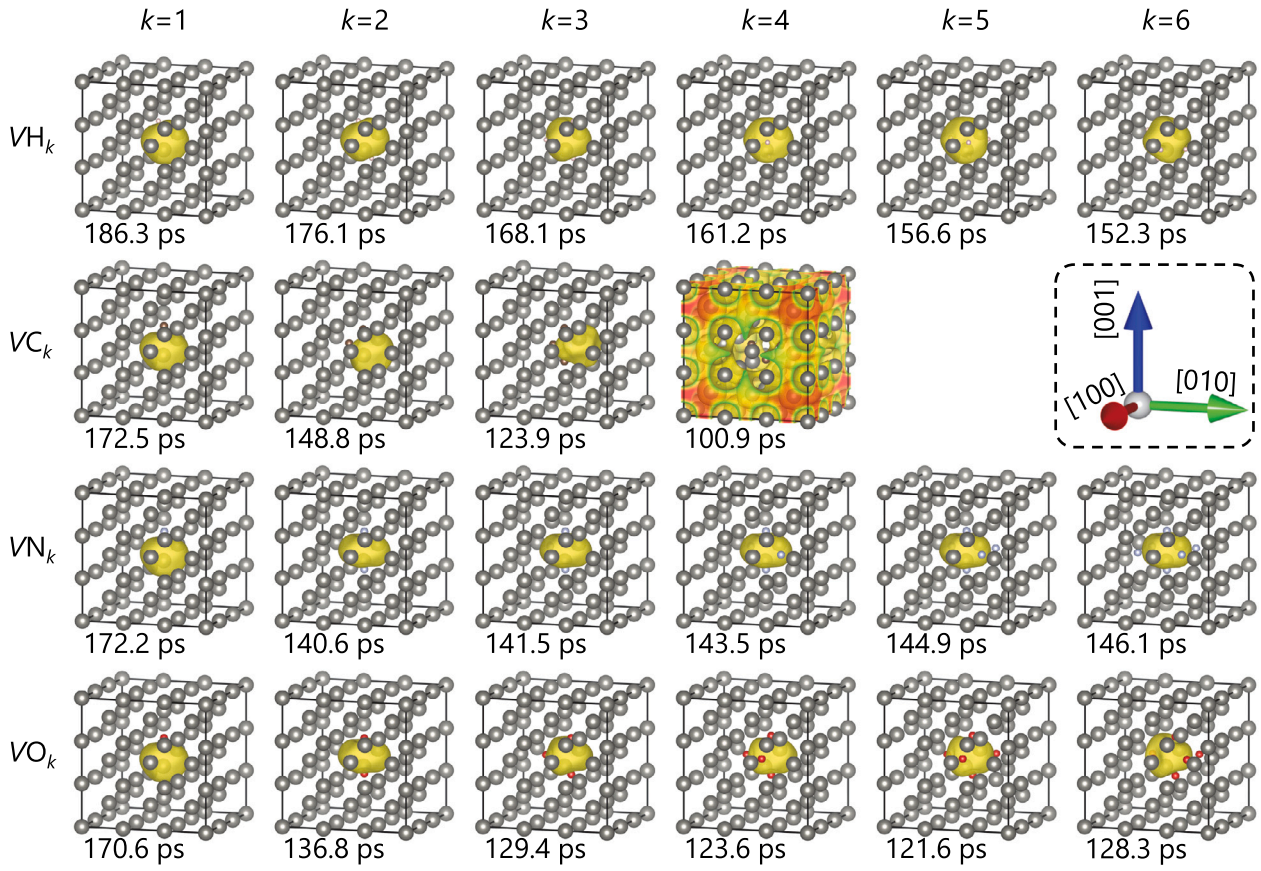

Fig. 10. Calculated positron density distributions for VH_k, VC_k, VN_k, and VO_k defect complexes. The calculated positron lifetimes obtained in this study are also indicated at the bottom of each panel. Note that the positron density distribution for the VC_4 defect complex, where a positron is delocalized, is emphasized compared with those for the other defect complexes.

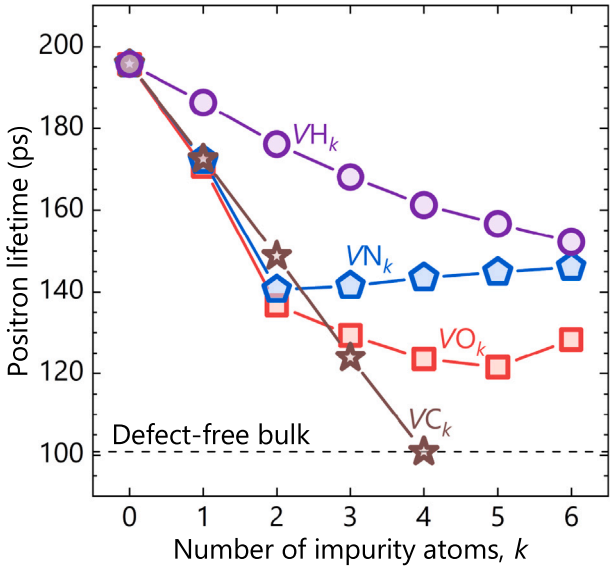

Fig. 11. Calculated positron lifetimes for isolated monovacancy ($k = 0$) and vacancy-impurity complexes. The calculated positron lifetime for defect-free bulk is also depicted as a dashed line.

to 172.5 ps. The positron lifetime of the VC_k defect complex showed a linear shortening trend with increasing k. In the VC_3, the localized positron is extruded by the three C atoms and presents a rather distorted shape, as shown in Fig. 10. The calculation showed that when a monovacancy was bound with four C atoms, a positron was no longer localized. In contrast to the positron localization in the other defect complexes, the positron was not localized in the VC_4 defect complex, as shown in Fig. 10. The aggregation of the four C atoms as shown in Fig. 6 makes the vacancy no longer a potential well for a positron. Therefore, the value of the defect-free bulk is plotted as the positron lifetime of the VC_4 defect complex in Fig. 11.

With increasing k, in contrast to the VH_k and VC_k defect complexes, the positron lifetime did not monotonically shorten for the VN_k and VO_k defect complexes. The positron lifetime of VN_1 was 172.2 ps, and that of VN_2 became even shorter, 140.6 ps. Fig. 10 indicates that the localized positron in the VN_2 is considerably compressed by the upper and lower N atoms. However, the positron lifetime of VN_k increased slightly with increasing k for $k \geq 3$, and that of VN_6 became 146.1 ps. This is because, for $k \geq 3$, the N atoms were located at the 2NN O-sites and expanded the distance between the W–W atoms, thereby increasing the vacancy volume. The positron lifetime reflects the electron density around a positron [1–4]. The increase in the positron lifetimes observed from VN_3 to VN_6 is consistent with the expansion of the low-electron-density region at $k \geq 3$ seen in Fig. 6. The positron lifetime of VO_k showed a small decrease for $k \geq 3$, and when k reached 6, it turned to increase.

To clearly show the effect of the different binding positions of the interstitial impurity atoms on the positron lifetime of the vacancy, the distance from the vacancy to the kth impurity atom, L, is plotted in Fig. 14. All L were normalized compared with the distance from the vacancy center to the unrelaxed 1NN O-site (= $0.5a$). In the VH_k and VC_k defect complexes, the impurity atoms were always bound at the $L < 1$ position. This means that the impurity atoms are relaxed inward from the unrelaxed 1NN O-site. In contrast to the VH_k and

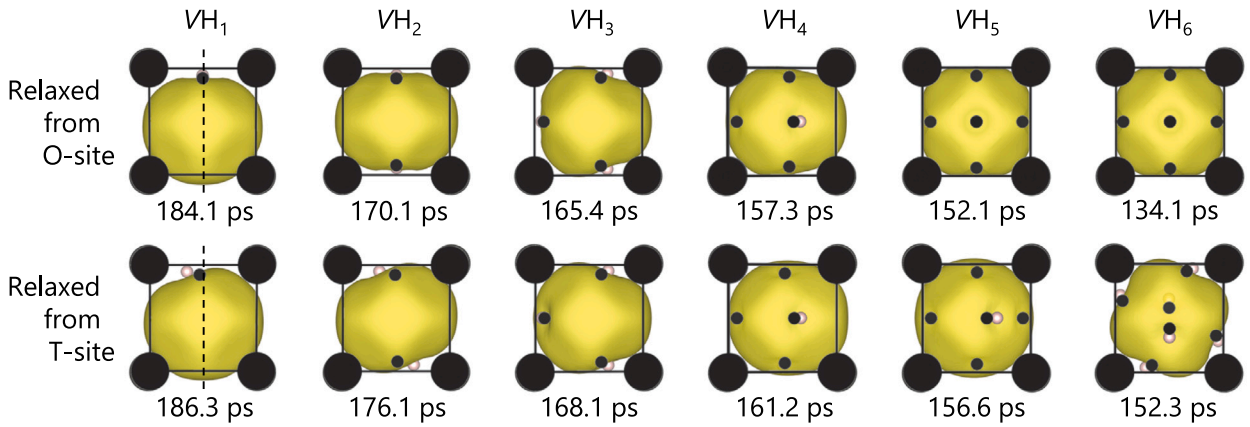

Fig. 12. Lattice relaxations of the VH_k defect complexes due to the positron localization. Black circles indicate atomic positions before positron localization. The upper and lower panels are atomic configurations obtained by relaxing the H atoms from the 1NN O-sites and T-sites, respectively. Dashed lines connecting the 1NN O-site and the vacancy center are also depicted in the VH_1 panels. The corresponding calculated positron lifetimes are indicated at the bottom of each panel.

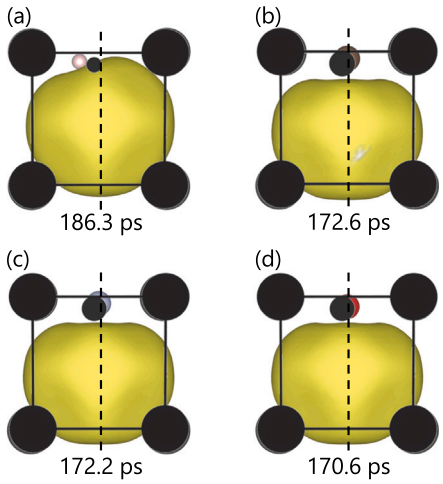

Fig. 13. Lattice relaxations of the (a) VH_1, (b) VC_1, (c) VN_1, and (d) VO_1 defect complexes due to the positron localization. Black circles indicate atomic positions before positron localization. The initial positions of C, N, and O atoms are located at the same position as the H atom. The corresponding calculated positron lifetimes are indicated at the bottom of each panel.

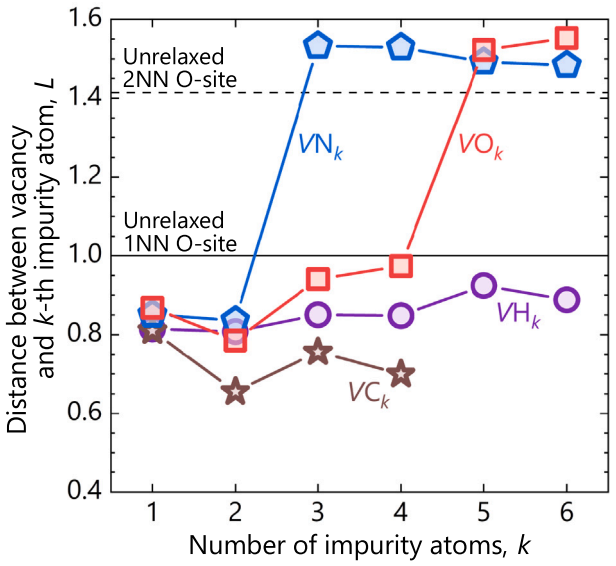

Fig. 14. Distance between vacancy and kth impurity atom, L. Each value is normalized compared with the distance from the vacancy center to the unrelaxed 1NN O-site ($= 0.5a$). The distances from the vacancy to the unrelaxed 1NN and 2NN O-sites are also depicted as solid and dashed horizontal lines, respectively.

VC_k defect complexes, Fig. 14 shows that in the VN_k and VO_k defect complexes, the impurity atoms sometimes bind to the outward of the unrelaxed 2NN O-site ($L > 1.414$). In the VN_k defect complex, the first and second N atoms also bound at $L < 1$ position, however, at $k \geq 3$ the N atoms were located outward of the unrelaxed 2NN O-site. Such binding of the interstitial impurity atoms away from the vacancy would have the effect of expanding the W lattice around the vacancy. The inverse change in positron lifetime observed in the VN_k and VO_k defect complexes is attributed to the different binding positions of the impurity atoms.

The calculations revealed that an increase in the number of interstitial impurity atoms binding to a vacancy did not monotonically shorten the positron lifetime in some cases. The position of the interstitial impurity atoms that bind to a vacancy affected the positron lifetimes of vacancy-impurity complexes. This is an effect that requires attention in identifying defect species from positron lifetimes.

4. Conclusion

In this study, first-principles calculations were performed for defect complexes consisting of a monovacancy and single or multiple interstitial impurity atoms (H, C, N, or O atoms) in W. The most stable atomic configurations of the vacancy-impurity complexes, the binding energies of an interstitial impurity atom to a vacancy (or vacancy-impurity complex), and the positron lifetimes at such defect complexes were calculated. For each defect complex, the most energetically stable atomic configuration was investigated. To this end, all atomic configurations were considered, where the impurity atom was located at the 1NN and 2NN O-sites from the vacancy. In calculating the positron lifetimes, the two-component DFT scheme was used, considering the effect of positron localization on the electron density distribution. Furthermore, the lattice relaxation associated with positron localization was taken into account to calculate the positron lifetimes.

For a couple of defect complexes, atomic configurations more stable than those reported (or probably assumed) in other studies were proposed. With the findings of more stable atomic configurations, more accurate binding energies of impurity atoms to vacancy-impurity complexes were also derived. In calculating positron lifetimes, slight deviations in the initial positions of the H atoms were found to be enhanced by positron localization, which affected the positron lifetimes

of the VH_k defect complexes. In addition, in contrast to the monotonically shortening positron lifetimes with increasing k at the VH_k and VC_k defect complexes, in some cases with increasing k, the positron lifetimes at the VN_k and VO_k defect complexes were increased. This means that attention must be paid to the identification of defect species from positron lifetimes. The inverse change in the positron lifetime observed in the VN_k and VO_k defect complexes was attributed to the binding of impurity atoms away from the vacancy.

CRediT authorship contribution statement

Atsushi Yabuuchi: Conceptualization, Methodology, Formal analysis, Resources, Writing – original draft, Writing – review & editing, Visualization, Funding acquisition.

Declaration of competing interest

The authors declare that they have no known competing financial interests or personal relationships that could have appeared to influence the work reported in this paper.

Data availability

Data will be made available on request.

Acknowledgments

This work was financially supported by Japan Society for the Promotion of Science (JSPS) KAKENHI grant number JP20K03902.

References

[1] R.W. Siegel, Positron annihilation spectroscopy, Annu. Rev. Mater. Sci. 10 (1980) 393, http://dx.doi.org/10.1146/annurev.ms.10.080180.002141.

[2] F. Tuomisto, I. Makkonen, Defect identification in semiconductors with positron annihilation: Experiment and theory, Rev. Modern Phys. 85 (2013) 1583, http://dx.doi.org/10.1103/RevModPhys.85.1583.

[3] J. Čížek, Characterization of lattice defects in metallic materials by positron annihilation spectroscopy: A review, J. Mater. Sci. Technol. 34 (2018) 577, http://dx.doi.org/10.1016/j.jmst.2017.11.050.

[4] F.A. Selim, Positron annihilation spectroscopy of defects in nuclear and irradiated materials- A review, Mater. Charact. 174 (2021) 110952, http://dx.doi.org/10.1016/j.matchar.2021.110952.

[5] P. Wilhartitz, R. Krismer, H. Hutter, M. Grasserbauer, S. Weinbruch, H.M. Ortner, 3D-SIMS analysis of ultra high purity molybdenum and tungsten: A characterisation of different manufacturing techniques and products, Fresenius' J. Anal. Chem. 353 (1995) 524, http://dx.doi.org/10.1007/BF00321315.

[6] A. Yabuuchi, M. Tanaka, A. Kinomura, Short positron lifetime at vacancies observed in electron-irradiated tungsten: Experiments and first-principles calculations, J. Nucl. Mater. 542 (2020) 152473, http://dx.doi.org/10.1016/j.jnucmat.2020.152473.

[7] K. Heinola, T. Ahlgren, Diffusion of hydrogen in BCC tungsten studied with first principle calculations, J. Appl. Phys. 107 (2010) 113531, http://dx.doi.org/10.1063/1.3386515.

[8] A. Alkhamees, Y.-L. Liu, H.-B. Zhou, S. Jin, Y. Zhang, G.-H. Lu, First-principles investigation on dissolution and diffusion of oxygen in tungsten, J. Nucl. Mater. 393 (2009) 508, http://dx.doi.org/10.1016/j.jnucmat.2009.07.012.

[9] X. Gonze, F. Jollet, F. Abreu Araujo, D. Adams, B. Amadon, T. Applencourt, C. Audouze, J.-M. Beuken, J. Bieder, A. Bokhanchuk, E. Bousquet, F. Bruneval, D. Caliste, M. Côté, F. Dahm, F. Da Pieve, M. Delaveau, M. Di Gennaro, B. Dorado, C. Espejo, G. Geneste, L. Genovese, A. Gerossier, M. Giantomassi, Y. Gillet, D.R. Hamann, L. He, G. Jomard, J. Laflamme Janssen, S. Le Roux, A. Levitt, A. Lherbier, F. Liu, I. Lukačević, A. Martin, C. Martins, M.J. T. Oliveira, S. Poncé, Y. Pouillon, T. Rangel, G.-M. Rignanese, A.H. Romero, B. Rousseau, O. Rubel, A.A. Shukri, M. Stankovski, M. Torrent, M.J. Van Setten, B. Van Troeye, M.J. Verstraete, D. Waroquiers, J. Wiktor, B. Xu, A. Zhou, J.W. Zwanziger, Recent developments in the ABINIT software package, Comput. Phys. Comm. 205 (2016) 106, http://dx.doi.org/10.1016/j.cpc.2016.04.003.

[10] X. Gonze, B. Amadon, G. Antonius, F. Arnardi, L. Baguet, J.-M. Beuken, J. Bieder, F. Bottin, J. Bouchet, E. Bousquet, N. Brouwer, F. Bruneval, G. Brunin, T. Cavignac, J.-B. Charraud, W. Chen, M. Côté, S. Cottenier, J. Denier, G. Geneste, P. Ghosez, M. Giantomassi, Y. Gillet, O. Gingras, D.R. Hamann, G. Hautier, X. He, N. Helbig, N. Holzwarth, Y. Jia, F. Jollet, W. Lafargue-Dit-Hauret, K. Lejaeghere, M.A. L. Marques, A. Martin, C. Martins, H.P. C. Miranda, F. Naccarato, K. Persson, G. Petretto, V. Planes, Y. Pouillon, S. Prokhorenko, F. Ricci, G.-M. Rignanese, A.H. Romero, M.M. Schmitt, M. Torrent, M.J. van Setten, B.V. Troeye, M.J. Verstraete, G. Zérah, J.W. Zwanziger, The ABINIT project: Impact, environment and recent developments, Comput. Phys. Comm. 248 (2020) 107042, http://dx.doi.org/10.1016/j.cpc.2019.107042.

[11] A.H. Romero, D.C. Allan, B. Amadon, G. Antonius, T. Applencourt, L. Baguet, J. Bieder, F. Bottin, J. Bouchet, E. Bousquet, F. Bruneval, G. Brunin, D. Caliste, M. Côté, J. Denier, C. Dreyer, P. Ghosez, M. Giantomassi, Y. Gillet, O. Gingras, D.R. Hamann, G. Hautier, F. Jollet, G. Jomard, A. Martin, H.P. C. Miranda, F. Naccarato, G. Petretto, N.A. Pike, V. Planes, S. Prokhorenko, T. Rangel, F. Ricci, G.-M. Rignanese, M. Royo, M. Stengel, M. Torrent, M.J. van Setten, B.V. Troeye, M.J. Verstraete, J. Wiktor, J.W. Zwanziger, X. Gonze, ABINIT: Overview and focus on selected capabilities, J. Chem. Phys. 152 (2020) 124102, http://dx.doi.org/10.1063/1.5144261.

[12] P.E. Blöchl, Projector augmented-wave method, Phys. Rev. B 50 (1994) 17953, http://dx.doi.org/10.1103/PhysRevB.50.17953.

[13] G. Kresse, D. Joubert, From ultrasoft pseudopotentials to the projector augmented-wave method, Phys. Rev. B 59 (1999) 1758, http://dx.doi.org/10.1103/PhysRevB.59.1758.

[14] J.P. Perdew, K. Burke, M. Ernzerhof, Generalized gradient approximation made simple, Phys. Rev. Lett. 77 (1996) 3865, http://dx.doi.org/10.1103/PhysRevLett.77.3865.

[15] J. Wiktor, G. Jomard, M. Torrent, M. Bertolus, Electronic structure investigation of energetics and positron lifetimes of fully relaxed monovacancies with various charge states in 3*C*-SiC and 6*H*-SiC, Phys. Rev. B 87 (2013) 235207, http://dx.doi.org/10.1103/PhysRevB.87.235207.

[16] J. Wiktor, G. Jomard, M. Torrent, Two-component density functional theory within the projector augmented-wave approach: Accurate and self-consistent computations of positron lifetimes and momentum distributions, Phys. Rev. B 92 (2015) 125113, http://dx.doi.org/10.1103/PhysRevB.92.125113.

[17] M.J. Puska, A.P. Seitsonen, R.M. Nieminen, Electron-positron Car-Parrinello methods: Self-consistent treatment of charge densities and ionic relaxations, Phys. Rev. B 52 (1995) 10947, http://dx.doi.org/10.1103/PhysRevB.52.10947.

[18] M. Mizuno, H. Araki, Y. Shirai, Theoretical calculations of positron lifetimes for metal oxides, Mater. Trans. 45 (2004) 1964, http://dx.doi.org/10.2320/matertrans.45.1964.

[19] K. Momma, F. Izumi, VESTA 3 for three-dimensional visualization of crystal, volumetric and morphology data, J. Appl. Crystallogr. 44 (2011) 1272, http://dx.doi.org/10.1107/S0021889811038970.

[20] K. Ohsawa, J. Goto, M. Yamakami, M. Yamaguchi, M. Yagi, Trapping of multiple hydrogen atoms in a tungsten monovacancy from first principles, Phys. Rev. B 82 (2010) 184117, http://dx.doi.org/10.1103/PhysRevB.82.184117.

[21] L. Sun, S. Jin, X.-C. Li, Y. Zhang, G.-H. Lu, Hydrogen behaviors in molybdenum and tungsten and a generic vacancy trapping mechanism for H bubble formation, J. Nucl. Mater. 434 (2013) 395, http://dx.doi.org/10.1016/j.jnucmat.2012.12.008.

[22] J.N. Mundy, Electrical resistivity-temperature scale of tungsten, Phil. Mag. A 46 (1982) 345, http://dx.doi.org/10.1080/01418618208239923.

[23] K.-D. Rasch, R.W. Siegel, H. Schultz, Quenching and recovery investigations of vacancies in tungsten, Phil. Mag. A 41 (1980) 91, http://dx.doi.org/10.1080/01418618008241833.

[24] K. Maier, M. Peo, B. Saile, H.E. Schaefer, A. Seeger, High-temperature positron annihilation and vacancy formation in refractory metals, Phil. Mag. A 40 (1979) 701, http://dx.doi.org/10.1080/01418617908234869.

[25] Y.-L. Liu, H.-B. Zhou, Y. Zhang, Investigating behaviors of H in a W single crystal by first-principles: From solubility to interaction with vacancy, J. Alloys Compd. 509 (2011) 8277, http://dx.doi.org/10.1016/j.jallcom.2011.03.117.

[26] K. Heinola, F. Djurabekova, T. Ahlgren, On the stability and mobility of di-vacancies in tungsten, Nucl. Fusion 58 (2018) 026004, http://dx.doi.org/10.1088/1741-4326/aa99ee.

[27] D. Nguyen-Manh, A.P. Horsfield, S.L. Dudarev, Self-interstitial atom defects in BCC transition metals: Group-specific trends, Phys. Rev. B 73 (2006) 020101, http://dx.doi.org/10.1103/PhysRevB.73.020101, (R).

[28] S.-C. Lee, J.-H. Choi, J.G. Lee, Energetics of He and H atoms with vacancies in tungsten: First-principles approach, J. Nucl. Mater. 383 (2009) 244, http://dx.doi.org/10.1016/j.jnucmat.2008.09.017.

[29] X.-C. Li, F. Gao, G.-H. Lu, Molecular dynamics simulation of interaction of H with vacancy in W, Nucl. Instrum. Methods Phys. Res. B 267 (2009) 3197, http://dx.doi.org/10.1016/j.nimb.2009.06.065.

[30] X.-S. Kong, Y.-W. You, C. Song, Q.F. Fang, J.-L. Chen, G.-N. Luo, C.S. Liu, First principles study of foreign interstitial atom (carbon, nitrogen) interactions with intrinsic defects in tungsten, J. Nucl. Mater. 430 (2012) 270, http://dx.doi.org/10.1016/j.jnucmat.2012.07.008.

[31] D. Nguyen-Manh, Ab-initio modelling of point defect-impurity interaction in tungsten and other BCC transition metals, Adv. Mater. Res. 59 (2009) 253, http://dx.doi.org/10.4028/www.scientific.net/AMR.59.253.

[32] Y.-L. Liu, H.-B. Zhou, S. Jin, Y. Zhang, G.-H. Lu, Dissolution and diffusion properties of carbon in tungsten, J. Phys.: Condens. Matter 22 (2010) 445504, http://dx.doi.org/10.1088/0953-8984/22/44/445504.

[33] Y.-L. Liu, H.-B. Zhou, Y. Zhang, G.-H. Lu, G.-N. Luo, Interaction of C with vacancy in W: A first-principles study, Comput. Mater. Sci. 50 (2011) 3213, http://dx.doi.org/10.1016/j.commatsci.2011.06.003.

[34] K. Sato, A. Hirosako, K. Ishibashi, Y. Miura, Q. Xu, M. Onoue, Y. Fukutoku, T. Onitsuka, M. Hatakeyama, S. Sunada, T. Yoshiie, Quantitative evaluation of hydrogen atoms trapped at single vacancies in tungsten using positron annihilation lifetime measurements: Experiments and theoretical calculations, J. Nucl. Mater. 496 (2017) 9, http://dx.doi.org/10.1016/j.jnucmat.2017.09.002.

[35] A. Alkhamees, H.-B. Zhou, Y.-L. Liu, S. Jin, Y. Zhang, G.-H. Lu, Vacancy trapping behaviors of oxygen in tungsten: A first-principles study, J. Nucl. Mater. 437 (2013) 6, http://dx.doi.org/10.1016/j.jnucmat.2013.01.317.

[36] T. Troev, E. Popov, P. Staikov, N. Nankov, T. Yoshiie, Positron simulations of defects in tungsten containing hydrogen and helium, Nucl. Instrum. Methods Phys. Res. B 267 (2009) 535, http://dx.doi.org/10.1016/j.nimb.2008.11.045.

[37] P. Staikov, N. Djourelov, Simulations of ⟨100⟩ edge and 1/2⟨111⟩ screw dislocations in α-iron and tungsten and positron lifetime calculations, Phys. B 413 (2013) 59, http://dx.doi.org/10.1016/j.physb.2012.12.026.